Multi-Objective Design Optimization of the Leg Mechanism for a Piping Inspection Robot

Renaud Henry, Damien Chablat, Mathieu Porez, Frédéric Boyer, Daniel Kanaan

▶ **To cite this version:**

Renaud Henry, Damien Chablat, Mathieu Porez, Frédéric Boyer, Daniel Kanaan. Multi-Objective Design Optimization of the Leg Mechanism for a Piping Inspection Robot. Proceedings of the ASME 2014 International Design Engineering Technical Conferences & Computers and Information in Engineering Conference, Aug 2014, Buffalo, United States. pp.1-10. hal-01008793

HAL Id: hal-01008793
https://hal.science/hal-01008793

Submitted on 17 Jun 2014

HAL is a multi-disciplinary open access archive for the deposit and dissemination of scientific research documents, whether they are published or not. The documents may come from teaching and research institutions in France or abroad, or from public or private research centers.

L'archive ouverte pluridisciplinaire **HAL**, est destinée au dépôt et à la diffusion de documents scientifiques de niveau recherche, publiés ou non, émanant des établissements d'enseignement et de recherche français ou étrangers, des laboratoires publics ou privés.

Proceedings of the ASME 2014 International Design Engineering Technical Conferences & Computers and Information in Engineering Conference
IDETC/CIE 2014
August 17-20, 2014, Buffalo, USA

DETC2014/MR-34593

MULTI-OBJECTIVE DESIGN OPTIMIZATION OF THE LEG MECHANISM FOR A PIPING INSPECTION ROBOT

Renaud HENRY, Damien CHABLAT,
Mathieu POREZ, Frédéric BOYER
Institut de Recherche en Communications et Cybernétique de Nantes (IRCCyN)
UMR CNRS n° 6597
1, rue de la Noë, 44321 Nantes Cedex 03, France
Email addresses:
{renaud.henry, damien.chablat}@irccyn.ec-nantes.fr
{mathieu.porez, frederic.boyer}@irccyn.ec-nantes.fr

Daniel KANAAN
AREVA NC, Bagnols sur Cèze, France
Email addresses: daniel.kanaan@areva.com

ABSTRACT

This paper addresses the dimensional synthesis of an adaptive mechanism of contact points ie a leg mechanism of a piping inspection robot operating in an irradiated area as a nuclear power plant. This studied mechanism is the leading part of the robot sub-system responsible of the locomotion. Firstly, three architectures are chosen from the literature and their properties are described. Then, a method using a multi-objective optimization is proposed to determine the best architecture and the optimal geometric parameters of a leg taking into account environmental and design constraints. In this context, the objective functions are the minimization of the mechanism size and the maximization of the transmission force factor. Representations of the Pareto front versus the objective functions and the design parameters are given. Finally, the CAD model of several solutions located on the Pareto front are presented and discussed.

INTRODUCTION

In a nuclear power plant, there are many places that the human workers cannot reach due to the high level of irradiation (which can be deadly). However, for safety reasons inherent to a nuclear power plant, the pipe-line equipments (which are large in such a plant) require periodic and rigorous inspections. In this context, the development of robotic system suitable to finding and to repaire a failure in such an environment is essential. It is for this reason, since many years, numerous articles appeared on this subject. In [1], the key issues raised by the design and the control of a piping inspection robot are presented. More generally, in the field of pipe inspections, four following major issues have to be faced: 1) how to move in a pipe; 2) how to locate in a pipe; 3) how to inspect a pipe area; 4) how to repair a default. Let us note that the work presented in our paper only deals with the first issue which falls within the locomotion issue. To achieve locomotion in such highly constrained pipe environment, we can classify the robot designs in two categories depending whether one takes inspiration from animals living in narrow spaces or from engineering knowledge and nine associated subcategories [2]. In the first category, we can imagine designs inspired from the earthworms [3], the snakes [4], the millipedes [5], the Lizards [6] and even from soft animals as the octopus [7]. For the second one, we find designs based on the using of wheels and pulleys [8], the telescopic [9], the impact [10] and the natural peristalsis [11]. The main problem of all these solutions is that each designed robot has a specific architecture for a given specification which is different in each case. Thus it is difficult to find the best architecture that responds to an user request. Despite this fact, the common denominators of all these

systems are the mechanisms to adapt the contact points of the robot on the pipe surface and those to generate the expected contact forces required by the desired motion in the pipe. It is in this context that this paper takes place. Thus, the aim of the paper is to design a mechanism able to adapt the contacts on the inner surface of a pipe under constraints inherent to the environment. More precisely, before defining the complete architecture of our piping robot, we want to find by an optimization into a mechanism selection, the best design minimizing the bulk volume of the robot and maximizing the transmission factor between the embedded motor and the contact points. To simplify, in this article, we call now such a system : the legs such as they are depicted in figure 1. In the context of our study, the considered pipe has a variable diameter between 28 mm and 58 mm with bends.

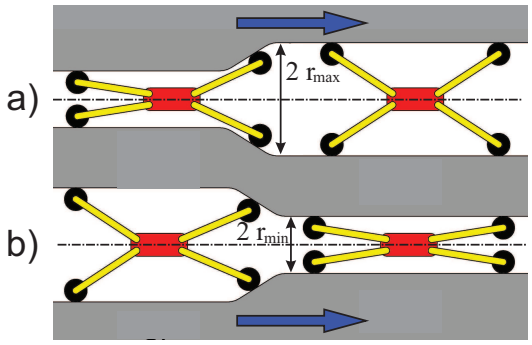

FIGURE 1. Piping robot with a generic adaptive mechanism of the contact points when the inner diameter: a) increases or b) decreases.

The outline of the paper is as follows. The mechanisms that we use to make the legs of our piping inspection robot are presented in first section. Then, the objective functions and the constraints on the design parameters are introduced. In section three, the optimization results under the form of Pareto fronts are presented. Moreover, CAD models of candidate mechanisms are shown. Finally, the article ends with a discussion and concluding remarks.

Locomotion and environment

The locomotion can be obtained either by putting actuated wheels or by varying the body length while the front and the rear part are alternately fixed to the pipe, the way worms do. These examples come from the classification made in [12] where seven categories of locomotion types as (i) the pig [13], (ii), the wheel [14], (iii) the crawler [15], (iv) the wall press [16], (v) the walking [17], (vi) the inchworm [18] and (vii) the screw type [19]. However, it is a well-known that the locomotion can be achieved in different ways according to the type of pipe: the wheels for the straight lines and the earthworms for the bends.

Before presenting the retained mechanisms, let us introduce some notations. Its inner radius of the pipe r varies between r_{min} and r_{max} with $r_{min} = 14$ mm and $r_{max} = 29$ mm.The minimum value is fixed in such a way that the robot can embedded a motor, electric and energy. Moreover, we define a reference frame whose the axis of motion, denoted by x, is along the main pipe axis and the motion of the mechanism under study is along the radius axis (Figure 1).

Geometric variations of piping

Park [20] lists a five principal geometric variations of piping. There are variations of (a) diameter, (b) curvature, and (c) inclination, (d) branched pipe, and (e) uneven inner surface. A pipe section can combine several geometric variations. For example we can have an inclined branched pipe with uneven inner surface. The variations of curvature limit the size of the robot when it negotiates the elbow [14]. There are four parameters to determine the size of the robot (1). The pipe have two parameters with the radius of piping r_p and the curvature r_c. The robot is defined in a cylinder with a diameter d_r and length l_r.

$$l_r = 2\sqrt{(2\,r_p - d_r)(2\,r_c + d_r)}\,. \tag{1}$$

So we choice a cylinder with a diameter of $d_r = 30$mm and a length of $l_r = 60$mm because the minus radius of curvature is $r_c = 45$ mm and radius of piping $r_p = 20$ mm.

Selection architectures of mechanism

We have selected two locomotion types, the inchworms . Then we have selected compatible mechanisms of locomotion types and geometric variations of piping. The three architectures of mechanism selected is a slot-follower mechanism [21–23], a crank and slider mechanism with 4 bars [12] and 6 bars [24]. Several mechanism have been removed. the solutions of Kawaguchi [25] have proposed magnetic wheels but the environment is nonmagnetic. Dertien [26] have built the Pirate robot for diameter range between 63 mm to 125 mm but the robot cannot be miniaturized and climb vertical pipe. Suzumori [27] have designed a micro inspection robot for recover an object in a 25 mm pipe, but drive system [28] is limited a small pipe diameter variation. Anthierens's thesis [29, 30] focuses on an inchworms locomotion in steam generator but variations and curvatures of diameter are not possible.

A slot-follower mechanism, a crank and slider mechanism with 4 bars and 6 bars

From the literature review, we have selected three architectures of mechanism suitable to be used according to the size of the pipe. For the three mechanisms, O is the origin of the reference frame, $P(x,y)$ is the coordinate of the end-effector and ρ is the length of the prismatic joint OA.

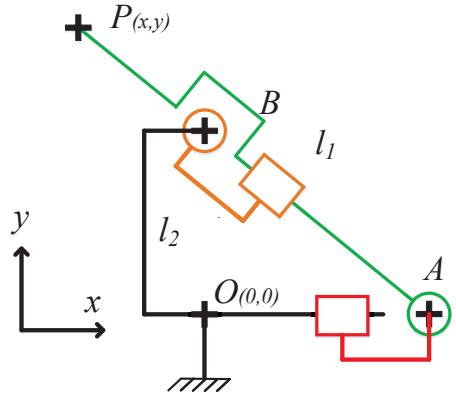

FIGURE 2. A slot-follower mechanism.

Figure 2 is a slot-follower mechanism [21–23] where the fixed prismatic joint is actuated and the other joints are idle. Lengths l_1 and l_2 denoting the lengths of AP and OB respectively define the geometry of mechanism entirely. The serial singularities (working mode changing) occur when the points A and O are coincided. The mechanical limits occur when the points P and B are coincided.

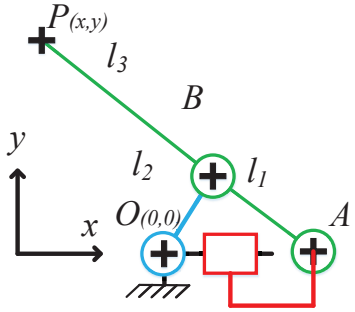

FIGURE 3. Crank and slider mechanism with 4 bars.

Figure 3 is a crank and slider mechanism with 4 bars [12] where the fixed prismatic joint is actuated and the other joints are idle. Lengths l_1, l_2 and l_3 denoting the lengths of AB, OB and BP respectively define the geometry of mechanism entirely. The parallel singularities occur when O, B and A are aligned.

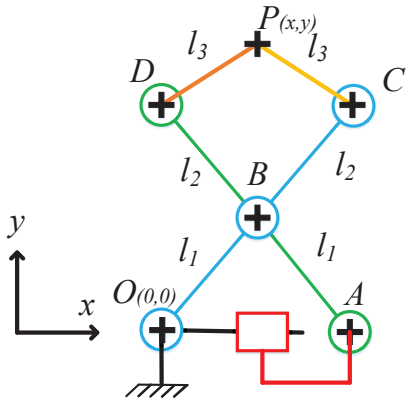

FIGURE 4. Crank and slider mechanism with 6 bars.

Figure 4 is a crank and slider mechanism with 6 bars [24] where one fixed prismatic joint is actuated and the other joints are idle. To reduce the design parameter space, we have added some equalities. Lengths l_1 denotes the lengths of AB and OB, lengths l_2 denotes the lengths of BD and BC and lengths l_3 denotes the lengths of DP and CP. These simplifications will be justified by the conclusion of the optimization of the crank and slider mechanism with 4 bars (See Section V). The parallel singularities occur when O, B and A are aligned or C, D and P are aligned.

Kinematic modeling of three mechanisms

The geometric parameters of the mechanism, l_1, l_2 , l_3 (only 4 bars and 6 bars mechanism) and the actuator displacements ρ permit us to define the Direct Kinematics Model (DKM) to have the relation between the geometric parameters of the mechanism, the actuator displacements and the moving platform pose y. The assembly mode is chosen such that $y > 0$ and $y > y_B$, where y_B is the ordinate coordinate of the point B. We also add constraints to avoid the singular configurations. The limits of y is defined by y_{max} and y_{min}. Figures 5–7 depict the three mechanisms in their lower, upper and intermediate configurations for the assembly mode chosen in the paper. The size of the mechanism is defined by Δx.

For a *slot-follower mechanism* (Figure 5), a single assembly mode exists and we have:

$$y = \frac{l_2 l_1}{\sqrt{{l_2}^2 + \rho^2}} \, . \tag{2}$$

The limits y_{max} and y_{min} are:

$$y_{min} = l_2 \text{ and } y_{max} = l_1 \, . \tag{3}$$

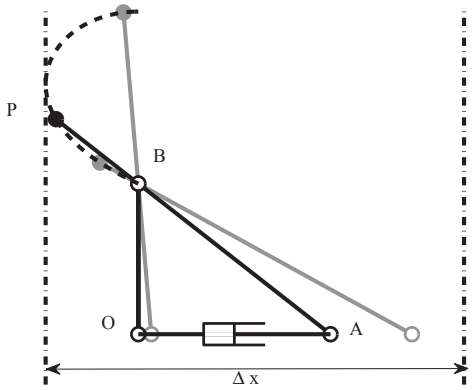

FIGURE 5. The black lines represent a slot-follower mechanism at an intermediate configuration. The gray lines correspond to the lower and upper configurations of the mechanism. The dotted line is the trajectory of P and Δx is the size of the mechanism.

y_{min} is constrained by the mechanical limits, when the points P and B are coincide and y_{max} is constrained by the length of l_1 in vertical, when the points A and O are coincide (Figure 5). As

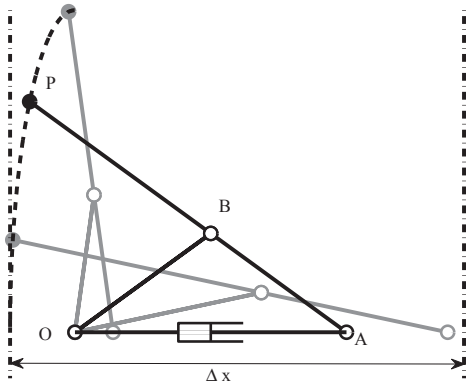

FIGURE 6. The black lines represent a Crank and slider mechanism with 4 bars at an intermediate configuration. The gray lines correspond to the lower and upper configurations of the mechanism. The dotted line is the trajectory of P and Δx is the size of the mechanism.

for a *crank and slider mechanism with 4 bars* (Figure 6), two assembly modes exist and we set

$$y = \frac{\sqrt{2l_1^2l_2^2 - l_1^4 + 2l_1^2\rho^2 - l_2^4 + 2\rho^2l_2^2 - \rho^4}\,(l_2 + l_3)}{2\rho l_2} \,. \qquad (4)$$

The limits y_{max} and y_{min} are:

$$y_{min} = 0 \text{ and } y_{max} = min\left(l_2\left(\frac{l_3}{l_1} + 1\right), l_1 + l_3\right) \,. \qquad (5)$$

y_{min} is zero when the mechanism is in parallel singularities because the points O, B and A are aligned.

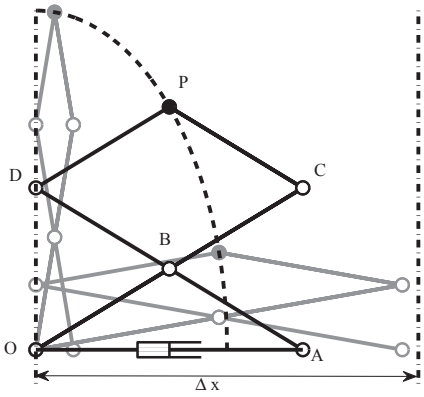

FIGURE 7. The black lines represent a Crank and slider mechanism with 6 bars at an intermediate configuration. The gray lines correspond to the lower and upper configurations of the mechanism. The dotted line is the trajectory of P and Δx is the size of the mechanism.

As for a *crank and slider mechanism with 6 bars* (Figure 7), four assembly modes exist and we set

$$y = \frac{\sqrt{a_1 + 2\sqrt{a_2}}}{2l_1} \,, \qquad (6)$$

with:

$$\begin{aligned} a_1 =& 4{l_1}^4 + 8{l_1}^3 l_2 + 4{l_1}^2{l_2}^2 + 4{l_1}^2{l_3}^2 - {l_1}^2\rho^2 \\ & - 2l_1 l_2 \rho^2 - 2{l_2}^2\rho^2 \,, \\ a_2 =& (2l_1 - \rho)(2l_1 + \rho)(l_1 + l_2)^2 \\ & (2l_1 l_3 - l_2\rho)(2l_1 l_3 + l_2\rho) \,. \end{aligned}$$

The limits y_{max} an y_{min} are:

$$y_{max} = l_1 + l_2 + l_3 \,, \qquad (7)$$

$$\text{if} \quad l_3 \geq l_2 \quad \text{then} \quad y_{min} = \sqrt{(l_3)^2 - (l_2)^2} \,, \qquad (8)$$

$$\text{else} \quad y_{min} = \sqrt{(l_2)^2 - (l_3)^2}\left(\frac{l_1}{l_2} + 1\right) \,. \qquad (9)$$

y_{max} is equal $l_1+l_2+l_3$ because the mechanism is in serial singularities when the all points are aligned in vertical. y_{min} is constrain by parallel singularities.

MULTI-OBJECTIVE DESIGN OPTIMIZATION

Objective functions

The multi-objective optimization problem aims to determine the optimum geometric parameters of the leg mechanism in order to minimize the size of the mechanism and to maximize the transmission factor.

Size of the mechanism There are numerous ways to define the compactness of a mechanism. The first objection function is

$$f_1 = \Delta x\,. \tag{10}$$

where Δx is the size of the mechanism on the x axis which is directly connected with the swept volume of the mechanism. Δx is obtained by the projection onto the x-axis of any points of the mechanism during its motion. We set:

$$\rho \geq 0.5 \text{ mm and } \Delta x \leq 35 \text{ mm}. \tag{11}$$

The first limit avoids the serial singularities [31] and the second one restricts the mechanism size.

Transmission force efficiency The second objective function is the transmission force efficiency which is defined as the ratio between output and input forces. We note

$$f_2 = \eta_f = \frac{F_w}{F_a}\,. \tag{12}$$

where F_a is the actuator force along the x axis, F_w is the contact force in P along the y axis and η_f is the transmission efficiency between the two forces. Moreover, for convenience, we set the transmission efficiency as follows:

$$\eta_f \geq 0.3\,. \tag{13}$$

In accordance with the definition of the transmission efficiency, for a *slot-follower mechanism*, we have:

$$\eta_f = \frac{\left(l_2{}^2+\rho^2\right)^{3/2}}{l_2\, l_1\, \rho}\,. \tag{14}$$

As regarding the *crank and slider mechanism with 4 bars*, we have:

$$\eta_f = 2\,\frac{\sqrt{-l_1{}^4+2\,l_1{}^2 l_2{}^2+2\,l_1{}^2\rho^2-l_2{}^4+2\,l_2{}^2\rho^2-\rho^4}\,\rho^2 l_2}{\left(l_2+l_3\right)\left(l_1{}^2-l_2{}^2+\rho^2\right)\left(LI^2-l_2{}^2-\rho^2\right)}\,. \tag{15}$$

Finally, for a *crank and slider mechanism with 6 bars*, we have:

$$\eta_f = 2\,\frac{l_1\,\sqrt{B}\sqrt{A}}{\rho\, C}\,, \tag{16}$$

with

$$\begin{aligned} A &= \left(2\,l_1-\rho\right)\left(2\,l_1+\rho\right)\left(l_1+l_2\right)^2\left(2\,l_3\,l_1-l_2\,\rho\right) \\ &\quad \left(2\,l_3\,l_1+l_2\,\rho\right)\,, \end{aligned} \tag{17}$$

$$\begin{aligned} B &= 4\,l_1{}^4+8\,l_1{}^3 l_2+4\,l_1{}^2 l_2{}^2-2\,l_2{}^2\rho^2+4\,l_3{}^2 l_1{}^2 \\ &\quad -l_1{}^2\rho^2-2\,l_1\,\rho^2 l_2+2\sqrt{A}\,, \end{aligned} \tag{18}$$

$$\begin{aligned} C &= 2\,l_2{}^2\sqrt{A}+l_1{}^2\sqrt{A}+2\,l_1\,l_2\,\sqrt{A}+4\,l_2{}^4 l_1{}^2 \\ &\quad +8\,l_2{}^3 l_1{}^3-2\,l_2{}^4\rho^2-2\,l_1{}^2 l_2{}^2\rho^2- \\ &\quad 4\,l_2{}^3\rho^2 l_1+4\,l_2{}^2 l_1{}^4+4\,l_3{}^2 l_1{}^4 \\ &\quad +8\,l_2\,l_3{}^2 l_1{}^3+4\,l_1{}^2 l_2{}^2 l_3{}^2\,. \end{aligned}$$

Design constraints

Due to assembly constraints, we have a set of inequalities. For a *slot-follower mechanism*, we have:

$$l_1 \geq r_{max} \text{ and } l_2 \leq r_{min}\,. \tag{19}$$

For a *crank and slider mechanism with 4 bars*, we have:

$$min\left(l_2\left(\frac{l_3}{l_1}+1\right), l_1+l_3\right) \geq r_{max} \text{ and } r_{min}=0. \tag{20}$$

For a *crank and slider mechanism with 6 bars*, we have:

$$l_1+l_2+l_3 \geq r_{max}\,, \tag{21}$$

$$\text{if} \quad l_2 \geq l_3 \quad \text{then} \quad \frac{\sqrt{l_2{}^2-l_3{}^2}}{l_2}\left(l_1+l_2\right) \leq r_{min}\,, \tag{22}$$

$$\text{else} \quad \sqrt{l_3{}^2-l_2{}^2} \leq r_{min}\,. \tag{23}$$

Design Variables

Along with the above mentioned geometric parameters l_1, l_2 and l_3 are considered as design variables, also called decision

variables. As there are three leg mechanisms under study, the leg type is another design variable that has to be taken into account. Let d denote the leg type: $d = 1$ stands for the slot-follower mechanism; $d = 2$ stands for crank and slider mechanism with 4 bars and $d = 3$ stands for the crank and slider mechanism with 6 bars. As a result, the optimization problem contains one discrete variable, *i.e.*, d, and three continuous design variables, *i.e.*, l_1, l_2, l_3. Hence, the design variables vector $\mathbf{x}$ is given by:

$$\mathbf{x} = [d, l_1, l_2, l_3]^T \tag{24}$$

Multi-objective optimization problem statement

The Multi-objective Optimization Problem (MOO) for a leg mechanism can be stated as: *Find the optimum design variables* $\mathbf{x}$ *of leg mechanism in order to minimize the size of the mechanism and maximize the transmission factor subject to geometric constraints.* Mathematically, the problem can be written as:

$$\begin{cases} \text{minimize } f_1(\mathbf{x}) = \Delta x \ ; \\ \text{maximize } f_2(\mathbf{x}) = \eta_f \ . \end{cases}$$

over $\quad \mathbf{x} = [d, l_1, l_2, l_3]^T$

subject to :

$$\begin{aligned}
g_1 &: \ l_1 \geq r_{max} \text{ for } d = 1 \ ; \\
g_2 &: \ l_2 \leq r_{min} \text{ for } d = 1 \ ; \\
g_3 &: \ min\left(l_2\left(\frac{l_3}{l_1}+1\right), l_1 + l_3\right) \geq r_{max} \text{ for } d = 2 \ ; \\
g_4 &: \ r_{min} \geq 0 \text{ for } d = 2 \ ; \\
g_5 &: \ l_1 + l_2 + l_3 \geq r_{max} \text{ for } d = 3 \ ; \\
g_6 &: \ \text{if} \quad l_2 \geq l_3 \quad \text{then} \quad \frac{\sqrt{{l_2}^2 - {l_3}^2}}{l_2}(l_1 + l_2) \leq r_{min} \\
&\quad \text{else} \quad \sqrt{{l_3}^2 - {l_2}^2} \leq r_{min} \text{ for } d = 3 \ ; \\
g_7 &: \ \eta_f \geq 0.3 \ ; \\
g_8 &: \ \rho \geq 0.5 \text{ mm} \ ; \\
g_9 &: \ \Delta x \leq 35 \text{ mm} \ ; \\
g_{10} &: \ 1 \text{ mm} \leq l_1, l_2, l_3 \leq 50 \text{ mm} \ .
\end{aligned}$$

Optimization implementation

The classic approach to optimization is to calculate all possible combinations in the solution space. With five settings (l_1,l_2,l_3,d,ρ), the computation time becomes excessive. For example, we have 12 billion combinations with 250 values for l_1,l_2,l_3,ρ and 3 values of d.

To solve the optimization problem, we use the genetic algorithm of Matlab [32]. A genetic algorithm is a search heuristic that mimics the process of natural selection. The computation time per mechanism is 2 hours with the settings:

- population size: 6000;
- pareto fraction: 50%;
- tolerance function: 10^{-4};
- number of sessions per problem: 5.

To scan the solution space, the algorithm uses a population of 6000 individuals with 50% of individuals on the Pareto front. This allows the other half of the population to reach other optimal solutions. For the same reason, we execute five sessions per mechanism in order to have redundancy. To reduce the computation time, tolerance precision of the objectives functions is 10^{-4}. The computer use an Intel Core i5-560 at 2.67GHz with 8 Go RAM.

RESULTS AND DISCUSSIONS

Based on the kinematic models introduced in section III, the multi-objective optimization problem, expressed in section IV, is solved by means MAPLE and MATLAB. MAPLE codes given the expression of the objective functions and MATLAB code provides functions for the optimization and to make filter to obtain the Pareto front. Figure 8 depicts the Pareto front obtained after the optimization.

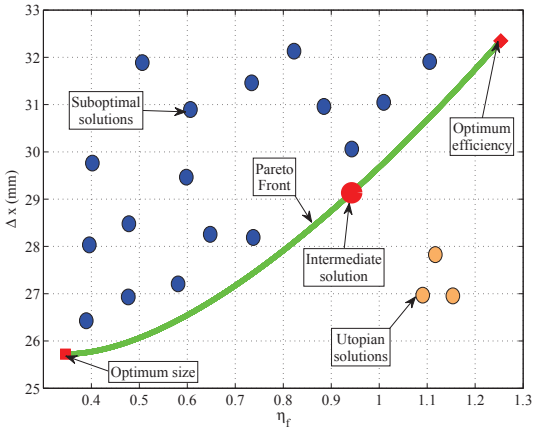

FIGURE 8. Example of the Pareto front with a mechanism versus the two objective functions Δx and η_f. The Pareto front includes optimal solutions. The suboptimal solutions are feasible but inferior to the Pareto front. Utopian solutions are to better than optimal solutions but infeasible.

To allow a better understanding of the Pareto front, we made

three optimizations by setting d = 1, 2, 3, *i.e.* the type of mechanism, as is depicted in Figure 9.

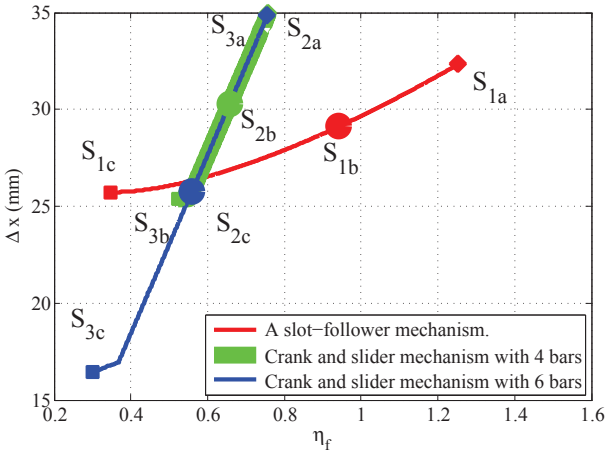

FIGURE 9. Pareto front associated with the three mechanisms with the two objective functions Δx and η_f.

Slot-follower mechanism

From the Pareto front, we can extract three values:

- optimum value of $\Delta x = 25.7$ mm with $\eta_f = 0.35$:

$$l_1 = 29.2 \text{ mm and } l_2 = 3.9 \text{ mm} ; \quad (25)$$

- optimum value of $\eta_f = 1.25$ with $\Delta x = 32.3$:

$$l_1 = 29.0 \text{ mm and } l_2 = 14.0 \text{ mm} ; \quad (26)$$

- intermediate solution $\Delta x = 29.1$ and $\eta_f = 0.94$:

$$l_1 = 29.0 \text{ mm and } l_2 = 10.5 \text{ mm} . \quad (27)$$

Figure 10 depicts the evolution of the design variables and Figure 11 the CAD model associated with the optimal value of Δx and η_f and an intermediate solution. We note that $l_2 = r_{min}$. Figure 12 depicts the evolution of the transmission force efficiency between the lower and upper configurations of the slot-follower mechanism. The constraint g_8 prevents a serial singularity. So the lever arm between points P, B and C intervenes. The value of transmission force efficiency is high for the optimum efficiency and Intermediate solutions because the length between P and B is small with $l_2 \approx r_{min}$. In contrast to the optimum size with a l_2 small.

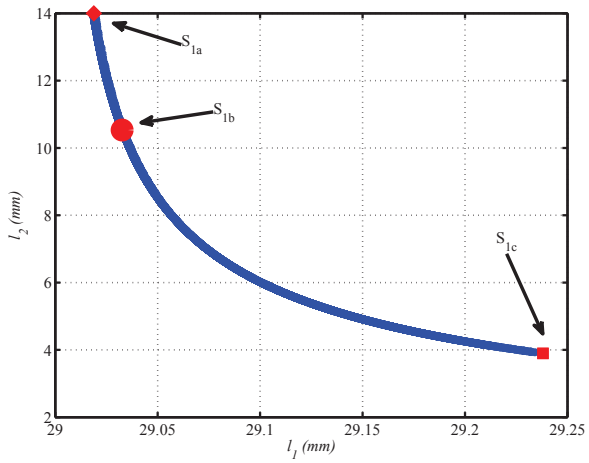

FIGURE 10. Pareto front for the slot-follower mechanism in the design parameter space. S_{1a} is an optimum efficiency solution, S_{1b} is an intermediate solution and S_{1c} is an optimum size solution.

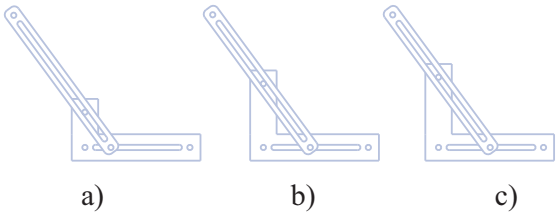

FIGURE 11. CAD model of the three solutions from the Pareto front for the slot-follower mechanism with a) the optimum size solution, b) the intermediate solution, c) the optimum efficiency solution.

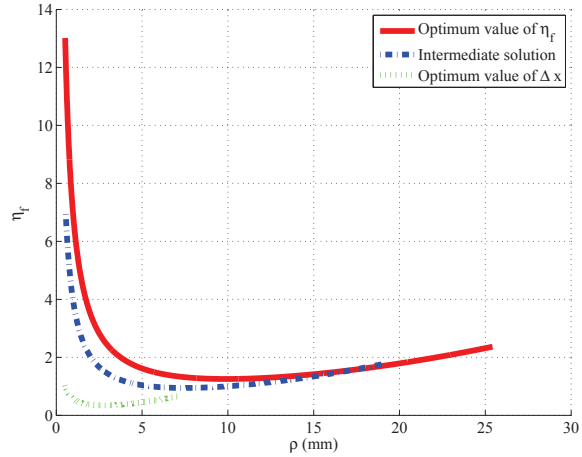

FIGURE 12. Evolution of the transmission force efficiency between the high and low position of the slot-follower mechanism.

Crank and slider mechanism with 4 bars

From the Pareto front, we can extract three values:

- optimum value of $\Delta x = 25.4mm$ with $\eta_f = 0.52$:

$$l_1 = 13.8 \text{ mm}, l_2 = 13.8 \text{ mm and } l_3 = 15.2 \text{ mm} ; \quad (28)$$

- optimum value of $\eta_f = 0.75$ with $\Delta x = 35.0mm$:

$$l_1 = 20.0 \text{ mm}, l_2 = 20.0 \text{ mm and } l_3 = 9.0 \text{ mm} ; \quad (29)$$

- intermediate solution $\Delta x = 30.3mm$ and $\eta_f = 0.65$:

$$l_1 = 17.3 \text{ mm}, l_2 = 17.3 \text{ mm and } l_3 = 11.7 \text{ mm} . \quad (30)$$

Figure 13 depicts the evolution of the design variables and Figure 14 the CAD model associated with the optimal value of Δx and η_f and an intermediate solution. We note that $l_1 = l_2$ and the Pareto front is defined by:

$$l_1 - 2\,l_2 - l_3 + 28.99 = 0 \quad (31)$$

The Pareto front is a straight line in the design parameter space of mechanism. The size of the mechanism is proportional in the length of l_1 and l_2. The transmission force efficiency is proportional in the length of l_3 because there is a lever arm between l_1 and l_3. If l_1 is smaller than l_3, the size of the mechanism is favoured. If l_3 is smaller than l_1, the transmission force efficiency is favored.

Crank and slider mechanism with 6 bars

From the Pareto front, we can extract three values:

- optimum value of $\Delta x = 16.4mm$ with $\eta_f = 0.30$:

$$l_1 = 8.8 \text{ mm}, l_2 = 8.8 \text{ mm and } l_3 = 11.6 \text{ mm} ; \quad (32)$$

- optimum value of $\eta_f = 0.75$ with $\Delta x = 34.9$:

$$l_1 = 19.8 \text{ mm}, l_2 = 4.6 \text{ mm and } l_3 = 4.6 \text{ mm} ; \quad (33)$$

- intermediate solution $\Delta x = 25.7mm$ and $\eta_f = 0.56$:

$$l_1 = 14.7 \text{ mm}, l_2 = 7.2 \text{ mm and } l_3 = 7.2 \text{ mm} . \quad (34)$$

Figure 15 depicts the evolution of the design variables and Figure 16 the CAD model associated with the optimal value of Δx

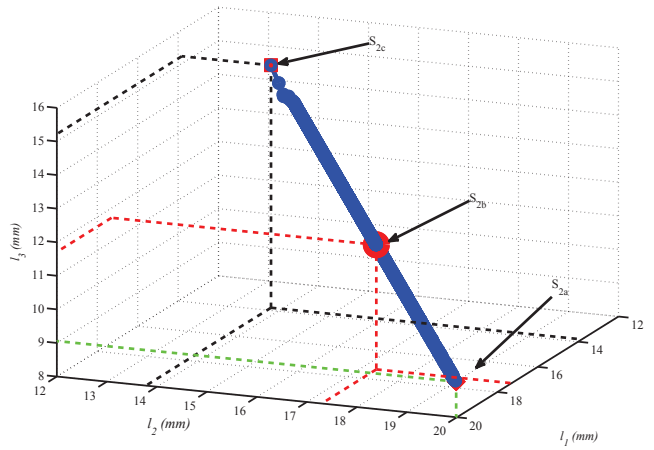

FIGURE 13. Pareto front for the crank and slider mechanism with 4 bars in the design parameter space. S_{2a} is an optimum efficiency solution , S_{2b} is an intermediate solution and S_{2c} is an optimum size solution .

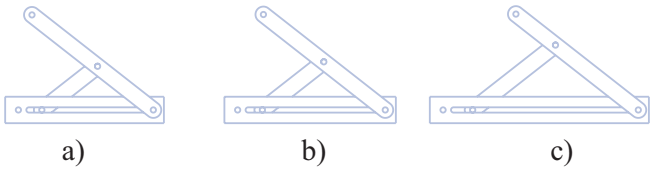

FIGURE 14. CAD model of the three solutions from the Pareto front for the Crank and slider mechanism with 4 bars a) the optimum size solution, b) the intermediate solution, c) the optimum efficiency solution.

and η_f and an intermediate solution.The Pareto front is defined by:

$$-l_1 - l_2 - l_3 + 29.04 = 0 \quad (35)$$

The first line of the Pareto front is without constraint g_9 and $l_2 = l_3$. The second line of the Pareto front with constraint g_9 and $l_1 = l_2$. The two lines are orthogonal. If we want to maximize the transmission force efficiency, we are in the case $l_2 = l_3$ (S_{3a}), so the ratio of the lever arm depends l_1/l_2. If we want to minimize the size of the mechanism, it is in the case $l_1 = l_2$ (S_{3c}), so the ratio of the lever arm depends l_2/l_3.

CONCLUSIONS

In this article, we have presented a multi-objective optimization problem to design the leg mechanisms of a pipe inspection robot. Three closed loop mechanisms are candidate to be used for the locomotion of this robot. We have defined two objective functions and a set of constraint equations related to the kine-

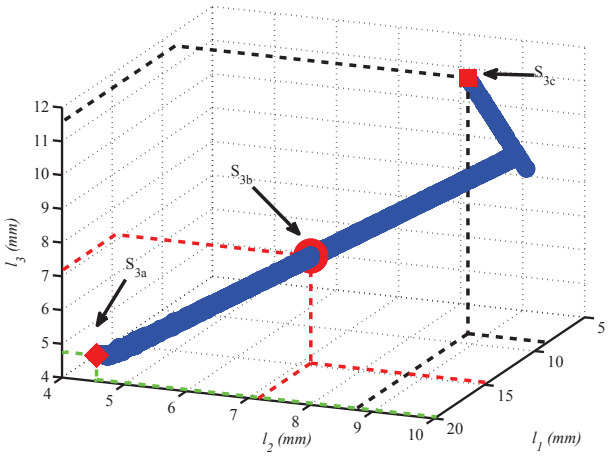

FIGURE 15. Pareto front for the crank and slider mechanism with 6 bars in the design parameter space. S_{3a} is an optimum efficiency solution , S_{3b} is an intermediate solution and S_{3c} is an optimum size solution .

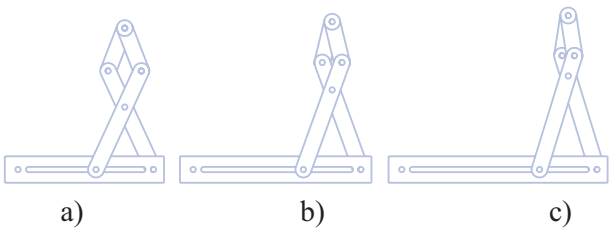

FIGURE 16. CAD model of the three solutions from the Pareto front for the Crank and slider mechanism with 6 bars a) the optimum size solution, b) the intermediate solution, c) the optimum efficiency solution.

matic behavior. A genetic algorithm is used to solve this problem with discrete and continuous variables. The optimization is made for each mechanism as three separate problems to explain the Pareto front obtained by the multi-objective problem resolution. We find out that the *slot-follower mechanism* is the best solution for a transmission force efficiency greater than 60% and the *Crank and slider mechanism with 6 bars* is the best for the other cases. We note that, for our constraint equations, the crank and slider mechanisms have similar performances. We select a S1a solution of slot-follower mechanism. The size of the mechanisms changes little between different solutions. The transmission force efficiency significantly changes between 60 % and 125 %. In a practical case, there will be at least 3 legs by groups. But The contact forces of legs is influenced by the cantilever between points 0, *P* and between two groups of legs. Similarly, dynamic phenomena are not taken into account in this paper. The transmission force efficiency is lower than for the slot-follower mechanism. Conversely, the slot-follower mechanism may be more difficult to build because of the passive prismatic and friction can reduce its efficiency. The mechanical strength of axes mechanisms may limit the transmitted power. In future works, the dynamic model with friction parameters will be used in locomotion phases to compare the efficiency of these mechanisms. Several locomotion pattern will be tested in our simulator to ensure contact between the robot and the inside surface of the pipe.

ACKNOWLEDGMENT

The work presented in this paper was partially funded by the AREVA company by and a grant of the Ecole des Mines de Nantes, France.

REFERENCES

[1] Kan Taguchi and Noriyuki Kawarazaki. Developement on in-pipe locomtion Robot. In *Advanced Robotics, 1991. 'Robots in Unstructured Environments', 91 ICAR., Fifth International Conference on*, pages 297 – 302 vol.1, 1991.

[2] I. Kassim, L. Phee, W. S. Ng, F. Gong, P. Dario, and C. A. Mosse. Locomotion techniques for robotic colonoscopy. *Engineering in Medicine and Biology Magazine*, 25(3):49–56, 2006.

[3] M. Drapier, V. Steenbrugghe, and B. Successeurs. Perfectionnements aux cathéters médicaux. *France Patent 1,278,965*, 1961.

[4] K. Ikuta, M. Tsukamoto, and S. Hirose. Shape memory alloy servo actuator system with electric resistance feedback and application for active endoscope, 1988.

[5] M. Utsugi. Tubular medical instrument having a flexible sheath driven by a plurality of cuffs. *U.S. Patent 4,148,307*, 1979.

[6] M. R. Treat and W. S. Trimmer. Self-propelled endoscope using pressure driven linear actuators. *US Patent 5,595,565*, 1997.

[7] I. Ginsburgh, J. A. Carlson, G. L. Taylor, and H. Saghatchi. Method and apparatus for fluid propelled borescopes. *U.S. Patent 4,735,501*, 1988.

[8] M. Takada. Self Propelled Colonoscope. *U.S. Patent 5,562,601*, 1996.

[9] S. Masuda. Apparatus for feeding a flexible tube through a conduit.

[10] J.M. Hyun, J.L. Hvung, M.L. Young, J.P. Juang, K. Byungkyu, and H.K. Soo. Magnetic impact actuator for robotic endoscope. In *Proc. 32nd Int. Symp. Robotics, Seoul, Korea*, pages 1834–1838, 2001.

[11] G.J. Iddan and D. Sturlesi. In-vivo video camera. *U.S. Patent 5,604,531*, pages U.S. Patent 5,604,531, 1997.

[12] S.-G. Roh and H. R. Choi. Differential-drive in-pipe robot for moving inside urban gas pipelines. *Transactions on Robotics*, 21(1):1–17, February 2005.

[13] J. Okamoto, J. C. Adamowski, M. S. G. Tsuzuki,

F. Buiochi, and C. S Camerini. Autonomous system for oil pipelines inspection. *Mechatronics*, 9(7):731–743, October 1999.

[14] H. R. Choi and S. Roh. In-pipe Robot with Active Steering Capability for Moving Inside of Pipelines. In *Bioinspiration and Robotics Walking and Climbing Robots*, chapter 23, pages 375–402. 2007.

[15] Y.-S. Kwon and B.-J. Yi. Design and motion planning of a two-moduled indoor pipeline inspection robot. *Transactions on Robotics*, 28(3):681–696, 2012.

[16] K. Tsuruta, T. Sasaya, T. Shibata, and N. Kawahara. Control Circuit in an In-Pipe Wireless Micm Inspection Robot. In *International Symposium on Micromechatronics and Human Science*, pages 59–64, Nagoya, Japan, 2000.

[17] W S.J. Phee, S. Ng, I.M. Chen, and F. Seow-Choen. Development of a Robotic Colonoscope. *Digestive Endoscopy*, 2(2):131–135, 2000.

[18] M. Ono and S. Kato. A Study of an Earthworm type Inspection Robot Movable in Long Pipes. *International Journal of Advanced Robotic Systems*, 7(1):85–90, 2010.

[19] M. Horodinca, I. Doroftei, E. Mignon, and A. Preumont. A simple architecture for in-pipe inspection robots. In *International Colloquium on Autonomous and Mobile Systems*, pages 1–4, Magdeburg, Germany, 2002.

[20] J. Park, D. Hyun, W.-H. Cho, T.-H. Kim, and H.-S. Yang. Normal-Force Control for an In-Pipe Robot According to the Inclination of Pipelines. *Transactions on Industrial Electronics*, 58(12):5304–5310, December 2011.

[21] P. Valdastri, R. J. Webster, C. Quaglia, M. Quirini, A. Menciassi, and P. Dario. A New Mechanism for Mesoscale Legged Locomotion in Compliant Tubular Environments. *Transactions on Robotics*, 25(5):1047–1057, 2009.

[22] B. Kim, H. Y. Lim, and K. D. Kim. A locomotive mechanism for a robotic colonoscope. In *International Conference on Intelligent Robots and Systems*, pages 1373 – 1378 vol.2, Lausanne, Switzerland, 2002.

[23] M. Quirini and R. J. Webster. Design of a pill-sized 12-legged endoscopic capsule robot. In *International Conference on Robotics and Automation*, pages 10–14, Roma, 2007.

[24] T. Okada and T. Sanemori. MOGRER: A vehicle study and realization for in-pipe inspection tasks. *Journal on Robotics and Automation*, 3(6):573–582, December 1987.

[25] Y. Kawaguchi, I. Yoshida, H. Kurumatani, T. Kikuta, and Y. Yamada. Internal pipe inspection robot. In *International Conference on Robotics and Automation*, pages 857 – 862 vol.1, Nagoya, Japan, 1995.

[26] E. Dertien, S. Stramigioli, and K. Pulles. Development of an inspection robot for small diameter gas distribution mains. In *International Conference on Robotics and Automation*, pages 5044–5049, Shanghai, May 2011.

[27] K. Suzumori, T. Miyagawa, M. Kimura, and Y. Hasegawa. Micro inspection robot for 1-in pipes. *Transactions on Mechatronics*, 4(3):286–292, 1999.

[28] T. Miyagawa and A. Configuration. Characteristics of In-pipe Mobile Robot with Wheel Drive Mechanism using Planetary Gears. In *International Conference on Mechatronics and Automation*, pages 3646–3651, Harbin, 2007.

[29] C. Anthierens, A. Ciftci, and M. Betemps. Design of an electro pneumatic micro robot for in-pipe inspection. In *International Symposium on Industrial Electronics*, pages 968–972, Bled, 1999.

[30] C. Anthierens, C. Libersa, M. Touaibia, M. Betemps, M. Arsicault, and N. Chaillet. Micro robots dedicated to small diameter canalization exploration. In *International Conference on Intelligent Robots and Systems*, pages 480–485, Takamatsu, 2000.

[31] D. Chablat and P. Wenger. Working modes and aspects in fully parallel manipulators. In *Robotics and Automation, . Proceedings. 1998 IEEE International Conference on*, volume 3, pages 1964–1969. IEEE, 1998.

[32] Raza Ur-Rehman, Stéphane Caro, Damien Chablat, and Philippe Wenger. Multiobjective Design Optimization of 3-PRR Planar Parallel Manipulators. In *20th CIRP Design conference*, pages 1–10, Nantes, France, 2010.